Investigating metabolic disease in human induced pluripotent stem cells : apidocyte size, insulin signaling and hepatic lipids

Friesen, M.

Biochemical and Biophysical Research Communications 495 (2018) 254–260

Contents lists available at ScienceDirect

Biochemical and Biophysical Research Communications

journal homepage: www.elsevier.com/locate/ybbrc

FPLD2 *LMNA* mutation R482W dysregulates iPSC-derived adipocyte function and lipid metabolism

Max Friesen [a, b], Chad A. Cowan [a, c, *]

[a] Division of Cardiovascular Medicine, Beth Israel Deaconess Medical Center, Boston, MA 02115, USA
[b] Department of Anatomy and Embryology, Leiden University Medical Center, 2300 RC, Leiden, The Netherlands
[c] Harvard Stem Cell Institute, Harvard University, Cambridge, MA 02138, USA

ARTICLE INFO

Article history:
Received 27 October 2017
Accepted 2 November 2017
Available online 3 November 2017

Keywords:
Adipocytes
Insulin resistance
Adipogenesis
Lipodystrophy
FPLD2

ABSTRACT

Lipodystrophies are disorders that directly affect lipid metabolism and storage. Familial partial lipodystrophy type 2 (FPLD2) is caused by an autosomal dominant mutation in the *LMNA* gene. FPLD2 is characterized by abnormal adipose tissue distribution. This leads to metabolic deficiencies, such as insulin-resistant diabetes mellitus and hypertriglyceridemia. Here we have derived iPSC lines from two individuals diagnosed with FPLD2, and differentiated these cells into adipocytes. Adipogenesis and certain adipocyte functions are impaired in FPLD2-adipocytes. Consistent with the lipodystrophic phenotype, FPLD2-adipocytes appear to accumulate markers of autophagy and catabolize triglycerides at higher levels than control adipocytes. These data are suggestive of a mechanism causing the lack of adipose tissue in FPLD2 patients.

1. Introduction

Mutations in the *LMNA* gene result in a family of syndromes known as laminopathies, including premature aging syndromes, myopathies, neuropathies, and lipodystrophy. *LMNA* lipodystrophy is known as familial partial lipodystrophy type 2 (FPLD2), an autosomal dominant genetic disorder [1]. FPLD2 is characterized by atypical subcutaneous adipose tissue distribution; specifically atrophy of subcutaneous adipose in the trunk and limbs, and excess accumulation of supraclavicular fat [2]. This dearth of subcutaneous adipose tissue drives systemic insulin resistance and hyperinsulinemia, potentiating progression to diabetes mellitus as well as hypertriglyceridemia followed by early atherosclerosis [3]. Reduced adiposity also leads to decreased serum concentrations of the adipokine adiponectin [4].

The *LMNA* gene resides on chromosome 1q21, encoding nuclear lamins A and C [5]. The most common variant of *LMNA* associated with FPLD2 is a missense mutation, R482W. The R482W mutation is solely associated with FPLD2; carriers display no disorders associated with other laminopathies [6]. The mutated residue lies in the C-terminal globular tail of lamin A where it does not alter the three-dimensional structure of the protein [7]. This mutation causes structural defects in the nuclear envelope as a result of disrupted protein-protein interactions [8,9].

We have reprogrammed induced pluripotent stem cell (iPSC) lines derived from individuals carrying the R482W mutation of *LMNA*. We differentiated the iPSCs into adipocytes (FPLD2-adipocytes) to investigate the cellular underpinnings of FPLD2. These *LMNA* R482W iPSC lines display reduced adipogenesis, altered insulin signaling as well as markers of increased autophagy. FPLD2-adipocytes exhibit increased basal and stimulated lipolysis as well as increased maximal mitochondrial activity. These molecular abnormalities in iPSC-derived adipocytes may be connected to the disease pathogenesis.

2. Results

2.1. Generating patient iPS lines

The aim of this study was to compare adipocytes derived from carriers of the *LMNA* R482W mutation with those of healthy controls (Fig. 1A). Towards this end we reprogrammed iPSCs from

* Corresponding author. Division of Cardiovascular Medicine, Beth Israel Deaconess Medical Center, Boston, MA 02115, USA.
E-mail addresses: maxfriesen@gmail.com (M. Friesen), chadacowan@gmail.com (C.A. Cowan).

https://doi.org/10.1016/j.bbrc.2017.11.008
0006-291X/

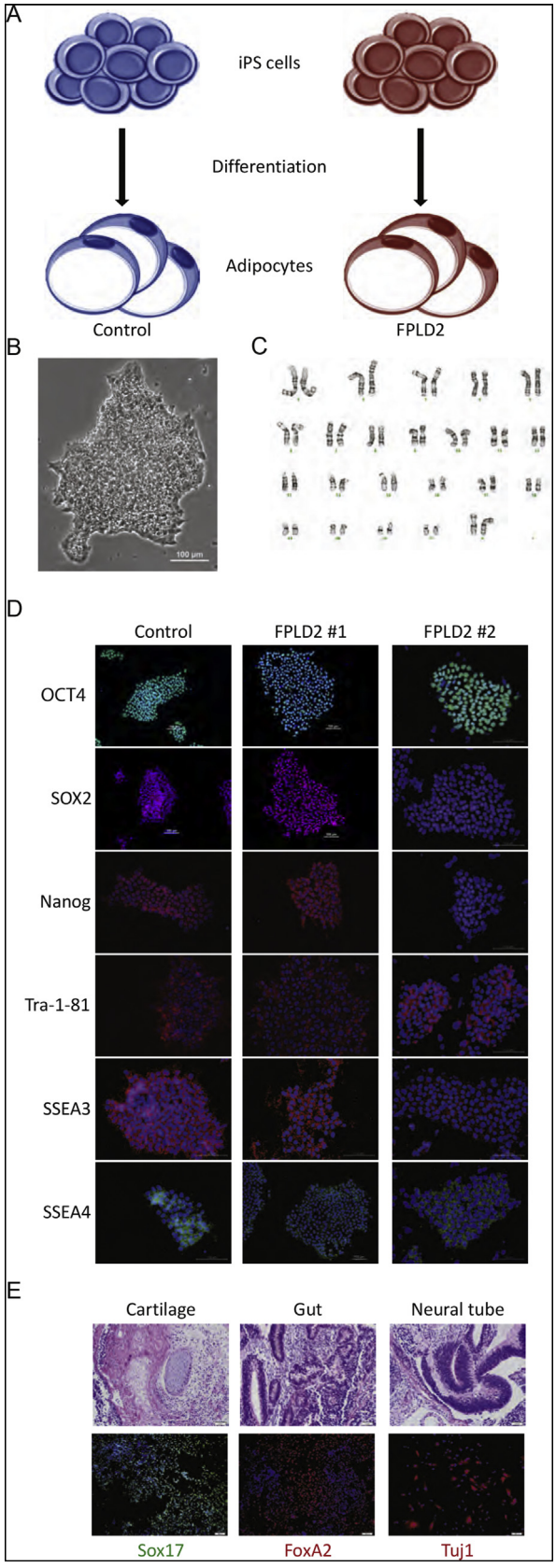

Fig. 1. iPS cell characterization. A) Experimental outline of the study. B) Representative iPS cell colony. C) Karyotype results of one of the FPLD2 lines. D) Immunostaining for pluripotency markers of the WT control line and both FPLD2 lines. E) Results of the teratoma assay exhibiting all three germ layers by H&E staining and immunofluorescence.

dermal fibroblasts obtained from two FPLD2 individuals harboring the R482W missense mutation in the *LMNA* gene. The cells displayed normal pluripotent stem cell morphology (Fig. 1B) and carried no chromosomal abnormalities (Fig. 1C). The cells also expressed pluripotency markers (OCT4, Nanog, Tra-1-81, SSEA3, and SSEA4) as evidenced by immunostaining (Fig. 1D). R482W FPLD2 iPSCs generated cells from all three germ layers in an *in vivo* teratoma formation assay, a hallmark of pluripotent cells (Fig. 1E).

2.2. FPLD2 lines have diminished capability for differentiation

Our previously established adipocyte differentiation protocol was employed to produce iPSC-derived white adipocytes (iPSC-WAT) [10]. Differentiation efficiency was evaluated by quantification of nuclei positive for the transcription factor and adipogenic master regulator CCAAT/Enhancer Binding Protein Alpha (C/EBP-alpha) [11]. Lipid droplets were imaged using a fluorescent neutral lipid dye (Fig. 2A). Both FPLD2-adipocytes and control cells were capable of adipogenesis, however the differentiation efficiency was decreased in the FPLD2 cell lines (Fig. 2B). Differentiated adipocytes also expressed the lipid droplet coating protein perilipin-1, while lamin A protein is detected in the nuclei of both FPLD2 and wild-type adipocytes (Fig. 2C). When partially differentiated cells were injected into the immunodeficient Rag2−/−;*Il2γC* mouse model, both groups of cells generated adipocytes. Adipocyte transplants were excised and imaged six weeks after implantation (Fig. 2D). Implants composed of control cells develop mature adipocytes with monolocular lipid droplets while the FPLD2 cells exhibited a disorganized structure and smaller lipid droplets.

2.3. FPLD2-adipocytes express decreased adipocyte markers and are resistant to insulin treatment

Correlating with decreased adipocyte differentiation, steady-state mRNA levels of mature adipocyte markers were also slightly decreased in FPLD2-adipocytes, including *AdipoQ, FABP4, HLS,* and *GLUT4* (Fig. 3A). To corroborate these findings we measured the cellular accumulation (Fig. 3B) and secretion (Fig. 3C) of adiponectin in FPLD2-adipocytes by immunoblotting and enzyme-linked immunosorbent assay (ELISA). Both of these measures indicated a significant reduction in adiponectin production, in agreement with decreased *ADIPOQ* gene expression. These findings are consistent with the clinical observation of reduced adiponectin in the serum of FPLD2 patients [4].

Next, we tested the response of these adipocytes to insulin stimulation. Phosphorylation of AKT and ERK1/2 in response to insulin appeared decreased in FPLD2-adipocytes (Fig. 3D and E). The reduced signal transduction downstream of the insulin receptor observed in *LMNA* R482W mutant cells requires additional investigation to determine the exact molecular basis, but is consistent with previous reports of insulin resistance in FPLD2 patients [3].

2.4. Functional deficiencies of FPLD2 adipocytes

Since the mechanism of fat loss in FPLD2 is not well understood, we performed lipolysis assays using iPSC-derived adipocytes. FPLD2-adipocytes displayed increased lipolysis both under basal conditions and during isoproterenol stimulation (Fig. 4A). Elevated lipolysis lead to increased fatty acid utilization by FPLD2-adipocyte mitochondria; and the observed maximal oxygen consumption rate was heightened in FPLD2-adipocytes (Fig. 4B).

Furthermore we investigated autophagic flux in iPSC-WAT. The observed ratio of LC3-II to LC3-I increased in the FPLD2 lines as measured by western blot, suggesting an increase in

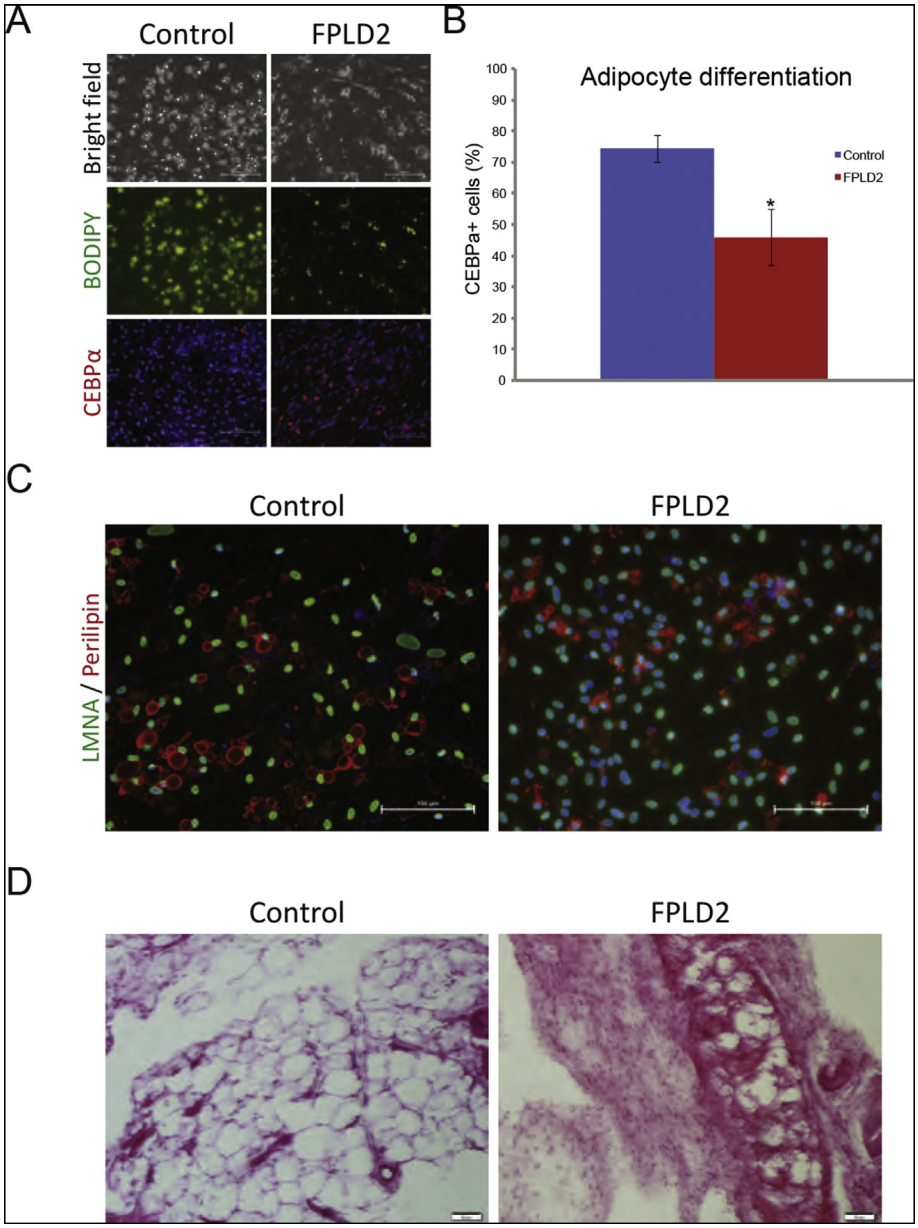

Fig. 2. Adipocyte differentiation and quality control. A) Brightfield imaging, BODIPY and CEBPα immunofluorescence of healthy and FPLD2 lines. DAPI is used as a nuclear co-stain. B) Quantification of the CEBPα-positive nuclei. C) Immunostaining of PLIN1 and LMNA. DAPI is used as a nuclear co-stain. D) Images of the adipose depots formed after injecting healthy or FPLD2 adipocytes into Rag2−/−;γC mice. Error bars, standard deviation. * = p-value ≤ 0.05.

autophagosome formation (Fig. 4C and D). Concomitantly, the steady-state protein level of the autophagy marker *ATG7* was increased in FPLD2 lines as measured by ELISA (Fig. 4E).

3. Discussion

The *LMNA* R482W mutation appears to manifest a number of cellular and molecular defects in iPSC-derived adipocytes. The clinical hallmarks of FPLD2 are lipoatrophy in the subcutaneous adipose depots of the limbs and trunk, insulin resistance, and decreased serum adiponectin levels [3,4]. FPLD2-iPSC lines are capable of adipocyte differentiation, albeit at a lower efficiency than control iPSC lines. Reduced differentiation efficiency is coupled with reduced mRNA expression of adipocyte markers. In accord with the clinical phenotype, adiponectin accumulation and secretion are significantly reduced in FPLD2-adipocytes. Additionally, insulin-dependent phosphorylation of AKT2 and ERK1/2 was impaired in FPLD2-adipocytes, which could explain the insulin resistance in FPLD2 adipocytes. These cellular phenotypes recapitulate several key clinical phenotypes observed in FPLD2 patients.

The reduction of adipose tissue in FPLD2 *in vivo* could be driven by a combination of increased lipolysis and decreased lipogenesis, as observed in this study. Elevated lipolysis in FPLD2-adipocytes liberates free fatty acids from intracellular stores, providing the substrate for increased oxygen consumption. We speculate that the coupling of increased fatty acid catabolism with decreased *de novo* lipogenesis, normally driven by insulin signaling, may shift the lipid metabolism balance in FPLD2-adipocytes [12]. This shift in lipid

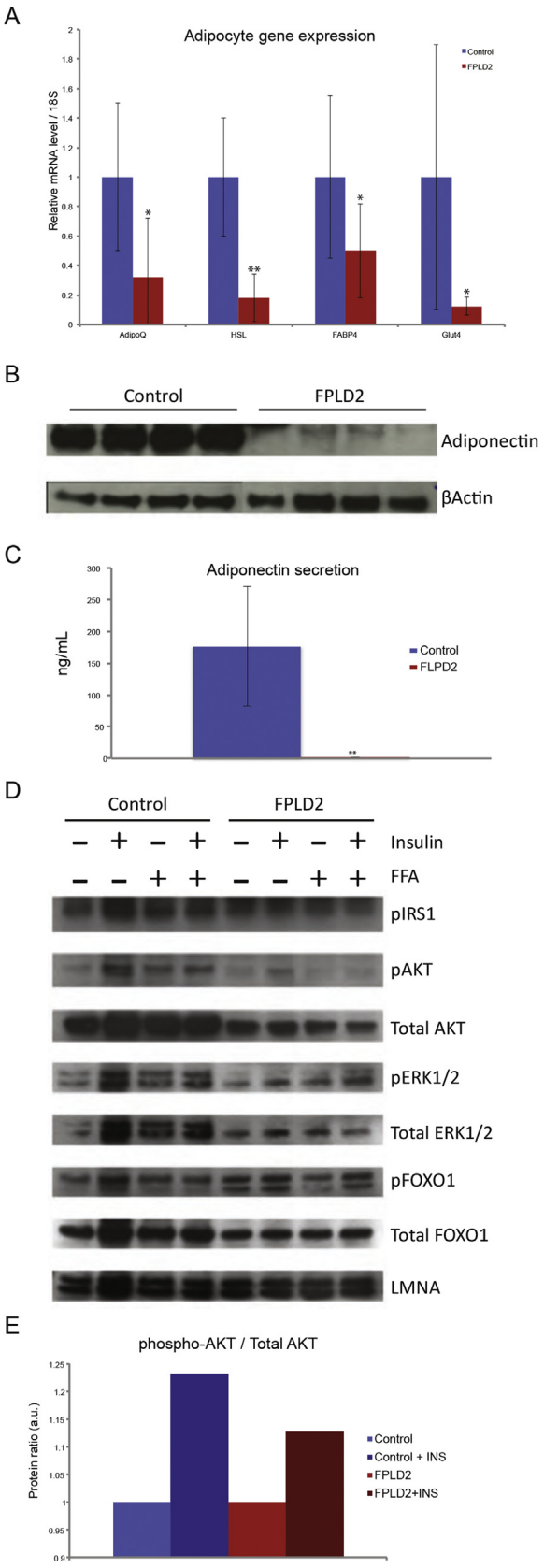

Fig. 3. FPLD2 adipocytes lack key adipocyte features and are insulin resistant. A) qPCR for *ADIPOQ*, *HSL*, *FABP4* and *GLUT4*, normalized to healthy lines and *18S* used as an internal control. B) Western blot for intracellular adiponectin protein. Beta-actin is used as a loading control. C) Adiponectin secretion from the adipocytes is measured by ELISA. D) Western blot for insulin signaling pathway proteins. Antibodies were used against phosphorylated IRS1, phosphorylated AKT, total AKT, phosphorylated ERK1/2, total ERK1/2, phosphorylated FoxO1, and total FoxO1. LMNA was used as a loading control. E) Ratio of phosphorylated over total AKT, data taken from panel D. Samples have been normalized by the loading control and differentiation efficiency. Error bars, standard deviation. * = p-value ≤ 0.05, ** = p-value ≤ 0.01.

metabolism could contribute to the observed localized lipoatrophy in FPLD2. Our data suggests that this metabolic shift towards fatty acid utilization may be coordinated by autophagy. Increased markers of autophagy in FPLD2-adipocytes are most parsimoniously explained via an upregulation of lipophagy or chaperone-mediated autophagy of perilipin, which would result in increased lipolysis [13–15].

4. Methods

4.1. iPS derivation

Human fibroblasts with LMNA mutations were provided by Dr. Vigouroux [18] and reprogrammed using retroviral vectors [19]. BJ RiPS were used as control iPS cell line [20].

4.2. Immunofluorescence

The following antibodies and dilutions were used: α-CEBPA 1:100 (Santa Cruz #sc-61), α-PLIN1 1:200 (Novus Biologicals), FABP4 (R&D Systems #PPS068), Oct4 (Santa Cruz #sc-8628), Nanog (Millipore #AB9220), Sox2 (Abcam #ab15830), SSEA3 (Millipore #MAB4303), SSEA4 (Millipore #MAB4304), Tra-1-81 (Millipore #MAB4381). Lipid droplets were stained using BoDIPY neutral lipid dye, cell nuclei with DAPI. Alexa Fluor secondary antibodies were used (Invitrogen). Images were acquired using a Nikon Eclipse Ti-S microscope. Both NIS-Elements and Image J software packages were used for image analysis.

After excision teratomas were formaldehyde-fixed, embedded in paraffin, sectioned and stained with hematoxylin and eosin, or with the following antibodies: FoxA2 (Abcam #ab40874), Sox17 (R&D Systems #AF1924), Tuj1 (Covance #MMS-435P).

4.3. Teratoma formation assay

The teratoma assay was performed as in Ref. [21].

4.4. In vivo adipocyte transplantation

Control or FPLD2 cells were differentiated for 14 days. Differentiated cells were injected subcutaneously into Rag2−/−;*Il2γC* mice from The Jackson Laboratory. Four weeks after transplantation, mice were killed to collect fat implants. Tissues at the transplantation site were formaldehyde-fixed, embedded in paraffin and hematoxylin and eosin stained after sectioning [22].

4.5. Adipocyte differentiation

Differentiation was performed as in Ref. [10]. Briefly, iPS cells were differentiated into mesenchymal progenitor cells (MPCs) through embryoid bodies. Lentiviral delivery of a doxycycline-inducible *PPARγ2* programmed the MPCs into mature white adipocytes.

4.6. Quantitative polymerase chain reaction (qPCR)

Total RNA from iPSC-adipocytes was extracted with Trizol (Invitrogen) and purified using the RNeasy mini kit (Qiagen) according to the manufacturer's instructions. The RNA yield was

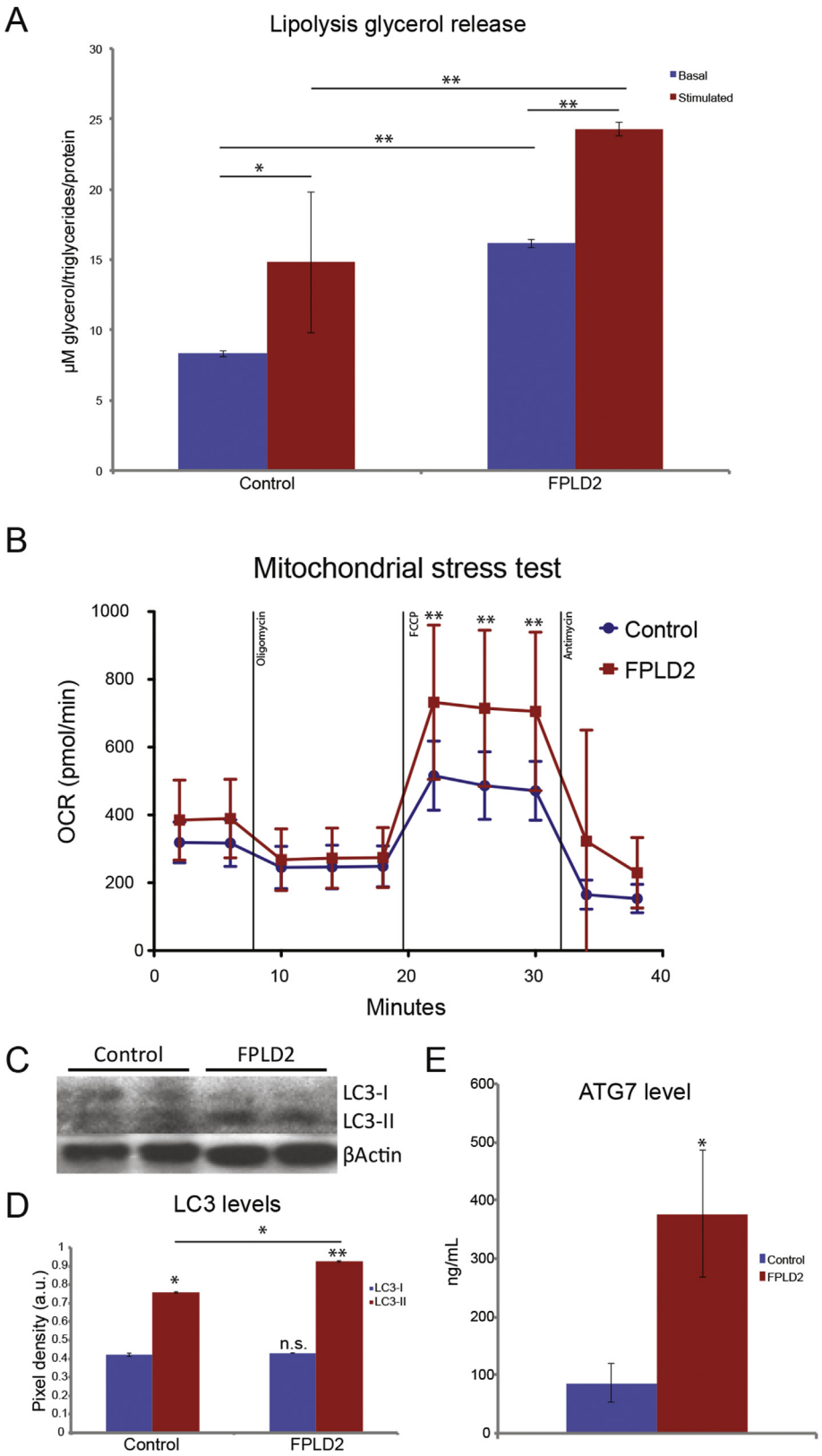

Fig. 4. FPLD2 adipocytes increase lipolysis as well as oxygen consumption and accumulate markers of autophagy. A) Lipolysis assay showing basal and isoproterenol-stimulated release of glycerol. B) Oxygen consumption during the mitochondrial stress test on a Seahorse XF analyzer. C) Western blot of LC3-I and LC3-II. Beta-actin is used as a loading control. D) Quantification of LC3 levels shown in panel C. E) ATG7 levels determined by ELISA. Error bars, standard deviation. * = p-value ≤ 0.05, ** = p-value ≤ 0.01.

determined using the NanoDrop ND-1000 spectrophotometer (NanoDrop Technologies). Total RNA (1 μg) was converted to cDNA using the Superscript First-Strand kit (Invitrogen). RT-qPCR was carried out using a Realplex Mastercycler (Eppendorf) with the Quantifast-SYBR Green PCR mix (Qiagen) with 1 μl cDNA per reaction. qPCR primer sequences used;

ADIPOQ:	F-gatgaagtcctgtcttggaagg	R-cagcacttagagatggagttgg.
GLUT4:	F-ccaacagataggctccgaaga	R-accgcagagaacacagcaa.
HSL:	F-gcctcagttccgaaaacca	R-cacccaggcggaagtctc.
FABP4:	F-tcatgaaaggcgtcacttcc	R-gcttgctaaatcagggaaaaca.
18S:	F-accgcagctaggaataatgga	R-gcctcagttccgaaaacca.

4.7. Western blotting

Adipocytes were starved overnight in DMEM containing 2% fatty acid free BSA. To induce insulin resistance, FFA mixture (lauric, myristic, linolein, oleic and arachidonic acids from Sigma) was used at 1 mM for 1 h. Insulin stimulation was carried out at 100 nM for 20 min. Cells were lysed in cold RIPA buffer (60 mM Tris-HCl at pH 7.4, 150 mM NaCl, 0.25% SDS and 1% NP40) containing 10 mM NaF, 1 mM Na3VO4 and complete protease inhibitor (Roche). Western blot analysis was carried out using the following antibodies: total AKT (Cell Signaling #9272), phospho-Ser-473 AKT (Cell Signaling #9271), phospho-IRS1 (Millipore #07-247), IRS1 (Santa Cruz #sc-559), Adiponectin (Abcam #ab22554), Beta-actin (Sigma #A5316), and lamin A/C (Fisher/Millipore #3211). Densitometry was performed using the gel analysis function of the ImageJ software package [23].

4.8. ELISA

Culture media was collected and ELISA was performed on a Luminex 200 analyzer using the Adiponectin or ATG7 ELISA kit (Millipore) following the manufacturer's instructions. ELISA readings from culture media alone were subtracted from each experimental sample as a background control, and protein concentration was used to normalize.

4.9. Lipolysis

To measure lipolysis activity, day 21 adipocytes differentiated from both healthy and FPLD2 iPSCs were starved in DMEM containing 1% FBS for 1 h. Cells were then incubated in HBSS (Hank's balanced salt solution) with 2% fatty-acid-free BSA alone, with 1–10 μM isoproterenol. The culture medium was collected for glycerol measurement using the free glycerol reagent (Sigma #F6428). Protein concentrations used to normalize glycerol content were measured using the Bradford protein assay (BioRad). Glycerol release was expressed in micrograms of glycerol per milligram of total protein.

4.10. Measurement of cellular oxygen consumption rate

Cells were plated in 0.1% gelatin-coated XF 24-well cell culture microplates (Seahorse Bioscience) and differentiated into adipocytes. Cells were incubated in pre-warmed unbuffered DMEM medium (DMEM containing 2 mM GlutaMAX, 1 mM sodium pyruvate, 1:85 g/L NaCl and 25 mM glucose) for 1 h. The oxygen consumption was measured by the XF24 extracellular flux analyzer (Seahorse Biosciences). Oxidative capacity was profiled by injecting perturbation drugs, 2 μM oligomycin, 0.5 μM FCCP (carbonyl cyanide-p-trifluoromethoxyphenylhydrazone) and 5 μM antimycin A, in succession. OCR was determined by plotting the oxygen tension of the medium in the chamber as a function of time.

Acknowledgments

This work was supported by NIH [Grant number - 5R01DK095384-03] ,NIDDK RO1-DK095384-05.

Transparency document

Transparency document related to this article can be found online at https://doi.org/10.1016/j.bbrc.2017.11.008.

References

[1] M.G. Dunnigan, M.A. Cochrane, A. Kelly, J.W. Scott, Familial lipoatrophic diabetes with dominant transmission. A new syndrome, Q. J. Med. 43 (1974) 33–48.
[2] S.A. Al-Attar, R.L. Pollex, J.F. Robinson, B.A. Miskie, R. Walcarius, C.H. Little, et al., Quantitative and qualitative differences in subcutaneous adipose tissue stores across lipodystrophy types shown by magnetic resonance imaging, BMC Med. Imaging 7 (2007) 3, https://doi.org/10.1186/1471-2342-7-3.
[3] A. Garg, Adipose tissue dysfunction in obesity and lipodystrophy, Clin. Cornerstone 8 (2006) S7–S13, https://doi.org/10.1016/S1098-3597(06)80039-6.
[4] W.A. Haque, I. Shimomura, Y. Matsuzawa, A. Garg, Serum Adiponectin, Leptin Levels, In patients with lipodystrophies, J. Clin. Endocrinol. Metabol. (2009), https://doi.org/10.1210/jcem.2002.87.issue-5;journal:journal:jcem;-website:website:endo;pageGroup:string:Publication.
[5] K.L. Wydner, J.A. McNeil, F. Lin, H.J. Worman, J.B. Lawrence, Chromosomal assignment of human nuclear envelope protein genes LMNA, LMNB1, and LBR by fluorescencein SituHybridization, Genomics 32 (1996) 474–478, https://doi.org/10.1006/geno.1996.0146.
[6] S. Shackleton, D.J. Lloyd, S.N.J. Jackson, R. Evans, M.F. Niermeijer, B.M. Singh, et al., LMNA, encoding lamin A/C, is mutated in partial lipodystrophy, Nat. Genet. 24 (2000) 153–156, https://doi.org/10.1038/72807.
[7] S. Dhe-Paganon, E.D. Werner, Y.I. Chi, S.E. Shoelson, Structure of the globular tail of nuclear lamin, J. Biol. Chem. 277 (2002) 17381–17384, https://doi.org/10.1074/jbc.C200038200.
[8] I. Krimm, C. Östlund, B. Gilquin, J. Couprie, P. Hossenlopp, J.-P. Mornon, et al., The Ig-like structure of the C-Terminal domain of lamin A/C, mutated in muscular dystrophies, cardiomyopathy, and partial lipodystrophy, Structure 10 (2002) 811–823, https://doi.org/10.1016/S0969-2126(02)00777-3.
[9] C. Capanni, Altered pre-lamin A processing is a common mechanism leading to lipodystrophy, Hum. Mol. Genet. 14 (2005) 1489–1502, https://doi.org/10.1093/hmg/ddi158.
[10] T. Ahfeldt, R.T. Schinzel, Y.-K. Lee, D. Hendrickson, A. Kaplan, D.H. Lum, et al., Programming human pluripotent stem cells into white and brown adipocytes, Nat. Cell Biol. 14 (2012) 209–219, https://doi.org/10.1038/ncb2411.
[11] E.D. Rosen, C.J. Walkey, P. Puigserver, B.M. Spiegelman, Transcriptional regulation of adipogenesis, Genes Dev. 14 (2000) 1293–1307, https://doi.org/10.1101/gad.14.11.1293.
[12] A.R. Saltiel, C.R. Kahn, Insulin signalling and the regulation of glucose and lipid metabolism, Nature 414 (2001) 799–806, https://doi.org/10.1038/414799a.
[13] S. Kaushik, A.M. Cuervo, Degradation of lipid droplet-associated proteins by chaperone-mediated autophagy facilitates lipolysis, Nat. Cell Biol. 17 (2015) 759–770, https://doi.org/10.1038/ncb3166.
[14] M. Schweiger, R. Zechner, Breaking the barrier—Chaperone-mediated autophagy of perilipins regulates the lipolytic degradation of fat, Cell Metab. 22 (2015) 60–61, https://doi.org/10.1016/j.cmet.2015.06.017.
[15] C. Ward, N. Martinez-Lopez, E.G. Otten, B. Carroll, D. Maetzel, R. Singh, et al., Autophagy, lipophagy and lysosomal lipid storage disorders, Biochimica Biophysica Acta (BBA) - Mol. Cell Biol. Lipids 1861 (2016) 269–284, https://doi.org/10.1016/j.bbalip.2016.01.006.
[18] A. Decaudain, M.-C. Vantyghem, B. Guerci, A.-C. Hécart, M. Auclair, Y. Reznik,

et al., New metabolic phenotypes in laminopathies: LMNA mutations in patients with severe metabolic syndrome, J. Clin. Endocrinol. Metabolism 92 (2009) 4835–4844, https://doi.org/10.1210/jc.2007-0654.
[19] I.-H. Park, R. Zhao, J.A. West, A. Yabuuchi, H. Huo, T.A. Ince, et al., Reprogramming of human somatic cells to pluripotency with defined factors, Nature 451 (2007) 141–146, https://doi.org/10.1038/nature06534.
[20] L. Warren, P.D. Manos, T. Ahfeldt, Y.-H. Loh, H. Li, F. Lau, et al., Highly efficient reprogramming to pluripotency and directed differentiation of human cells with synthetic modified mRNA, Cell Stem Cell. 7 (2010) 618–630, https://doi.org/10.1016/j.stem.2010.08.012.
[21] W.Y. Zhang, P.E. de Almeida, J.C. Wu, Teratoma formation: a tool for monitoring pluripotency in stem cell research, StemBook (2012), https://doi.org/10.3824/stembook.1.53.1.
[22] A.H. Fischer, K.A. Jacobson, J. Rose, R. Zeller, Hematoxylin and eosin staining of tissue and cell sections, Cold Spring Harb. Protoc. 2008 (2008), https://doi.org/10.1101/pdb.prot4986 pdb.prot4986–pdb.prot4986.
[23] M.D. Abràmoff, P.J. Magalhães, S.J. Ram, Image processing with ImageJ, Laurin Publishing, 2004.